INTERNATIONAL JOURNAL OF PRECISION ENGINEERING AND MANUFACTURING Vol. 15, No. 8, pp. 1657-1666 AUGUST 2014 / 1657
DOI: 10.1007/s12541-014-0516-5

Advanced Porous Scaffold Design using Multi-Void Triply Periodic Minimal Surface Models with High Surface Area to Volume Ratios

Dong-Jin Yoo[1,#]

1 Department of Computer Aided Mechanical Design Engineering, Daejin University, Pocheon, South Korea, 487-711
Corresponding Author / E-mail: djyoo@daejin.ac.kr, TEL: +82-31-539-2031, FAX: +82-31-539-1970

KEYWORDS: Surface area to volume ratio, Conventional TPMS scaffolds, Multi-void TPMS scaffolds, Multi-material TPMS tissue models, Additive manufacture, Organ printing

Creating biophysically and biologically desirable porous scaffolds has always been one of the greatest challenges in tissue engineering (TE). Advanced additive manufacture (AM) methods such as three-dimensional (3D) printing techniques have established remarkable improvements in the fabrication of porous scaffolds and structures close in architecture to biological tissue. Such fabrication techniques have opened new areas of research in TE. Recently, it was shown that porous scaffolds which are mathematically designed by using triply periodic minimal surface (TPMS) pore geometry and fabricated through 3D printing techniques have remarkably high cell viability and mechanical strength when compared with conventional scaffolds. The enhanced cell adhesion, migration, and proliferation of TPMS-based scaffolds arise from the high surface area to volume ratio (SA/V ratio) that is a basic and fundamental concept of biology. Here, we report the design of multi-void TPMS-based scaffolds that dramatically increase the SA/V ratio of conventional TPMS scaffolds. Our findings suggest that the proposed novel design methodology can be applied to create a variety of computational models for prototyping and printing of biomimetic scaffolds and bioartificial tissues.

Manuscript received: February 24, 2014 / Revised: April 14, 2014 / Accepted: April 16, 2014

NOMENCLATURE

$\phi_{Sphere\_scaffold\_three\_voids}$ = Distance field equation for a sphere-shaped scaffold model with three voids
$\phi_{Sphere\_scaffold\_four\_voids}$ = Distance field equation for a sphere-shaped scaffold model with four voids
ϕ_{Pore} = Distance field equation for the internal pore network of a multi-void scaffold
$\phi_{Support}$ = Distance field equation for the support pore architecture of a multi-void scaffold

1. Introduction

In order for cells to survive, they must constantly exchange ions, gases, nutrients, and wastes with their surrounding environment. These exchanges take place at the cell's surfaces. That is, a lot of biologically important things happen on cell's exterior surfaces. Therefore, the surface area to volume ratio abbreviated SA/V ratio has been a fundamental and significant biological concept. It is well known that SA/V ratio affects a variety of biological properties from the maximum size of a cell to the shape of an organ. SA/V ratio is formally defined as the amount of surface area per unit volume of an object. It is very important because so many biological functions happen on the surface of objects: (i) ions diffuse in and out of cells through channels and pores on their exterior surfaces; (ii) oxygen diffuses in and out of cells across their plasma membranes; (iii) heat diffuses out of our body through skin that covers our body surface. As an object grows in size, its surface area will grow too. For example, if a cell grows bigger, its internal volume enlarges and the cell's exterior surface expands. Unfortunately, the volume increases more rapidly than does the surface area, and so the relative amount of surface area available to pass materials to a unit volume of the cell steadily decreases. SA/V ratio affects more than just cells. It is important to large tissues or organs as well. Humans and other large animals cannot rely on diffusion to move oxygen and carbon dioxide directly in and out of their body. They must

have a transport system located to individual cells to transport the nutrients and wastes in and out. Most large animals have therefore specialized organs (i.e. lungs, kidneys, intestines, etc.) to increase the surface area available for exchange processes. For example, our lungs have numerous branches that lead to small thin grape-like sacs called alveoli. These increase the surface area for gas exchange in our lungs. Without the millions of sacs, our lungs would not have enough surface area to absorb all the oxygen we need.

In tissue engineering (TE), interior pore architecture of the porous scaffold is very important for the successful regeneration of tissues and organs. Hence, the design of the porous scaffold microarchitectures has always been one of the greatest challenges in TE. The advent of advanced fabrication techniques such as three-dimensional (3D) printing techniques has significantly improved control over the pore network and scaffold structures that mimic the intricate architecture and complexity of native tissues or organs. In recent years, to overcome the limitations of traditional computer-aided design (CAD) methods,[1-13] several researches started to use the triply periodic minimal surface (TPMS) pore geometry for designing the tissue engineering porous scaffolds.[14-24] The most important advantage of TPMS-based pore geometry compared with conventional CAD-based pore geometry is the precise and easy controllability of internal pore architectures, such as pore size, pore shape, porosity, interconnectivity, etc. Moreover the entire design process can be fully automated by a simple computer program. In addition, it was shown that the biologically and physically desirable TPMS-based pore geometry enhances cell migration and viability, while retaining a high degree of mechanical and structural rigidity. Hence, the TPMS-based pore geometry, possessing the advantages of both computational efficiency and enhanced interactions with cells, can be considered as one of the promising candidates for ideal pore geometries in the design of next generation scaffolds.

In fact, the enhanced cell adhesion, migration, and proliferation of TPMS-based scaffolds are directly related to the high surface area of TPMS pore architecture. As well as showing the easy controllability of pore architecture, TPMS-based scaffolds can provide high SA/V ratio because TPMSs are inherently smooth and continuous surfaces. An increased SA/V ratio means increased exposure to the environment. In other words, TPMS-based scaffolds have enough surface area for a sufficient amount of ions and oxygen to diffuse across. That is why TPMS-based scaffolds are so biologically desirable in terms of cell seeding, migration, and differentiation. As aforementioned, cells must constantly interact with their surrounding environment. As a cell grows bigger, its internal volume enlarges and the cell membrane expands. If there is not enough surface area available to service all the cells in the scaffold, the cells must stop growing. That is, if the cells in the scaffold grow beyond a certain limit, the cells will cease to function. In this point of view, the scaffold should provide a sufficient surface on which cells adhere, thrive, multiply, and generate the extracellular matrix (ECM) of structural and functional proteins that make up a living tissue. Therefore, high SA/V ratio is the most important requirement which a porous scaffold should have.

This paper proposes a new application method of TPMS in the field of porous scaffold design mainly focused on the multi-void TPMS pore architectures. The design method to be proposed in this work has two major advantages: (1) it is easy and efficient to design a sophisticated porous scaffold model with high SA/V ratio by introducing multi-void TPMS unit cell libraries, and (2) a variety of computational models for fabrication of scaffolds can be generated in the more general design framework. This paper is organized as follows. Section 2 illustrates a brief overview of TPMS and distance field (DF) absolutely necessary to explain the design methodology to be proposed in this work. Section 3 describes the procedure for the porous scaffold design using the multi-void TPMS. Several design examples are also illustrated. Finally, concluding remarks will be given in Section 4 along with some ideas for future research.

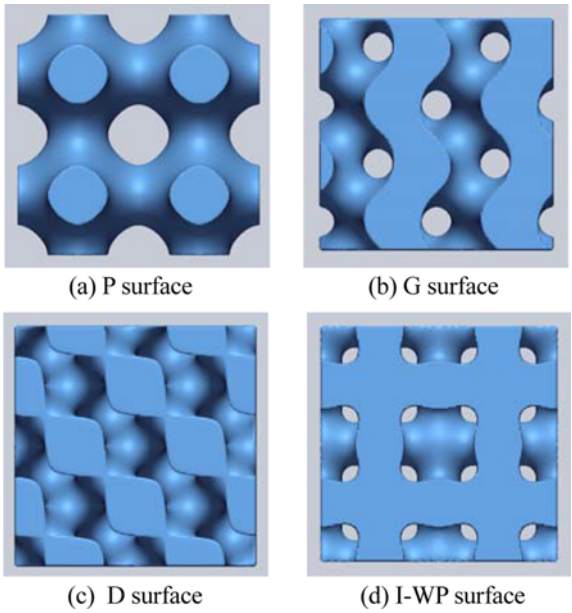

Fig. 1 TPMS-based unit cell libraries

2. TPMS and DF

2.1 TPMS

The biomorphic geometry that best mimics the tissue substrate would be one that is continuous through space and partitioned into two sub-spaces (cells and ECM) by a non-intersecting two-sided surface. TPMSs are ideal to describe such a biomimetic geometry.[14-31] As shown in Fig. 1, TPMSs are very smooth and continuous thereby resulting in optimized pore architectures with fully perfect pore interconnectivity and enhanced interactions with cells. A review of the many efficient methods for TPMS generation is beyond the scope of this paper. The reader may consult related works for more detailed informations.[17,18,32-37]

2.2 DF

The DF is an effective representation of a shape. Traditionally, DF is defined as a scalar field of distances to a shape. Each element in a DF specifies its minimum distance to the shape. Positive and negative distances are used to distinguish outside and inside of the shape, for example, using negative values on the outside and positive on the inside. A review of the many available methods for the efficient DF calculation and DF-based Boolean operations is beyond the scope of this paper. The reader may consult related works for more detailed

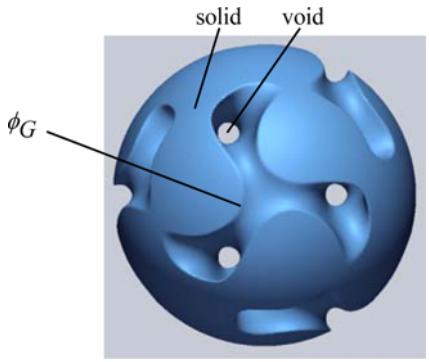

Fig. 2 A sphere-shaped scaffold model with one void

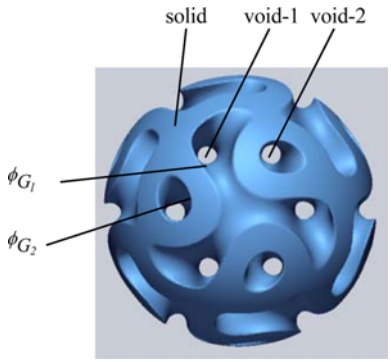

Fig. 3 A sphere-shaped scaffold model with two voids

informations.[18,20,22-24,38-41]

3. Proposed Algorithm for Multi-Void TPMS Scaffold Design

As aforementioned in our previous researches,[20,22] two types of scaffold pore architectures including minimal surface network solids and minimal surface sheet solids can be generated using the TPMS-based unit cell libraries.

A sphere-shaped network solid scaffold with G-surface unit cell library can be described as follows:

$$\phi_{Sphere\_scaffold\_one\_void} = \phi_{Sphere} \cap \phi_G = \min(\phi_{Sphere}, \phi_G) \tag{1a}$$

$$\phi_G = \sin(X)\cos(Y) + \sin(Z)\cos(X) + \sin(Y)\cos(Z) - C \tag{1b}$$

$$\phi_{Sphere} = x^2 + y^2 + z^2 - R^2 \tag{1c}$$

where R is the radius of sphere and ϕ_G is the TPMS G-surface. As shown in Fig. 2, the domain to one side of the TPMS represents the solid material, the other side the void domain. That is, the TPMS forms the solid/void interface and there is a single connected void domain.

In a similar way, a sphere-shaped sheet solid scaffold with G-surface unit cell library can be described as follows:

$$\begin{aligned}\phi_{Sphere\_scaffold\_two\_voids} &= \phi_{Sphere} \cap \phi_{G_1} \cap \phi_{G_2} \\ &= \min(\phi_{Sphere}, \min(\phi_{G_1}, \phi_{G_2}))\end{aligned} \tag{2a}$$

$$\phi_{G_1} = \sin(X)\cos(Y) + \sin(Z)\cos(X) + \sin(Y)\cos(Z) - C_1 \tag{2b}$$

$$\phi_{G_2} = -[\sin(X)\cos(Y) + \sin(Z)\cos(X) + \sin(Y)\cos(Z) - C_2] \tag{2c}$$

where ϕ_{G_1} and ϕ_{G_2} are the two TPMS surfaces inflated in both normal directions. As shown in Fig. 3, minimal surface sheet solid is a porous scaffold obtained by inflating the minimal surface to finite thickness. The solid domain separates two network-like void domains which are infinite and intertwined, but not interconnected. As noted by earlier researchers,[19] for technological applications where high porosity or minimal weight or resource consumption are the essential design targets, sheet solid scaffold (i.e., two-voids scaffold) represents the better solution superior to network solid scaffold (i.e., one-void scaffold). It is apparent that the reason for this result is mainly in the high SA/V ratio of two-voids scaffold when compared with that of one-void scaffold. As shown in Figs. 2 and 3, SA/V ratio is approximately proportional to the number of voids. That is, two-voids scaffold shows about two times higher SA/V ratio than the one-void scaffold due to the greater surface area for the same volume.

We further develop this idea to design a porous scaffold model with multi-void TPMS microarchitectures.

Let us consider a simple design example. To define a sphere-shaped scaffold model with three voids using G-surface unit cell library, the following operations can be applied:

$$\begin{aligned}\phi_{Sphere\_scaffold\_three\_voids} &= \phi_{Sphere} \cap (\phi_{Pore} \cup \phi_{Support}) \\ &= \min(\phi_{Sphere}, \max(\phi_{Pore}, \phi_{Support}))\end{aligned} \tag{3a}$$

$$\begin{aligned}\phi_{Pore} &= \phi_{G_0} \cap \phi_{G_3} - \phi_{G_1} \cap \phi_{G_2} \\ &= \min(\min(\phi_{G_0}, \phi_{G_3}), -\min(\phi_{G_1}, \phi_{G_2}))\end{aligned} \tag{3b}$$

$$\phi_{Support} = \phi_{G_1} \cap \phi_{G_2} \cap \phi_P = \min(\phi_P, \min(\phi_{G_1}, \phi_{G_2})) \tag{3c}$$

$$\phi_{G_0} = \sin(X)\cos(Y) + \sin(Z)\cos(X) + \sin(Y)\cos(Z) - C_0 \tag{3d}$$

$$\phi_{G_1} = \sin(X)\cos(Y) + \sin(Z)\cos(X) + \sin(Y)\cos(Z) - C_1 \tag{3e}$$

$$\phi_{G_2} = -[\sin(X)\cos(Y) + \sin(Z)\cos(X) + \sin(Y)\cos(Z) - C_2] \tag{3f}$$

$$\phi_{G_3} = -[\sin(X)\cos(Y) + \sin(Z)\cos(X) + \sin(Y)\cos(Z) - C_3] \tag{3g}$$

$$\phi_P = \cos(X) + \cos(Y) + \cos(Z) - C \tag{3h}$$

where ϕ_{G_0}, ϕ_{G_1}, ϕ_{G_2}, and ϕ_{G_3} are the four TPMS surfaces inflated in normal directions used in the definition of spatial limits of each void. Fig. 4 shows the application result of Eq. 3.

Theoretically, there is no limitation in the number of voids. To define a sphere-shaped scaffold model with four voids, the similar operations can be used as follows:

$$\begin{aligned}\phi_{Sphere\_scaffold\_four\_voids} &= \phi_{Sphere} \cap (\phi_{Pore} \cup \phi_{Support}) \\ &= \min(\phi_{Sphere}, \max(\phi_{Pore}, \phi_{Support}))\end{aligned} \tag{4a}$$

$$\begin{aligned}\phi_{Pore} &= \phi_{G_0} \cap \phi_{G_5} - \phi_{G_1} \cap \phi_{G_2} - \phi_{G_3} \cap \phi_{G_4} \\ &= \min(\min(\min(\phi_{G_0}, \phi_{G_5}), -\min(\phi_{G_1}, \phi_{G_2})), -\min(\phi_{G_3}, \phi_{G_4}))\end{aligned} \tag{4b}$$

$$\begin{aligned}\phi_{Support} &= (\phi_{G_1} \cap \phi_{G_2} \cap \phi_P) \cup (\phi_{G_3} \cap \phi_{G_4} \cap \phi_P) \\ &= \max(\min(\phi_P, \min(\phi_{G_1}, \phi_{G_2})), \min(\phi_P, \min(\phi_{G_3}, \phi_{G_4})))\end{aligned} \tag{4c}$$

$$\phi_{G_0} = \sin(X)\cos(Y) + \sin(Z)\cos(X) + \sin(Y)\cos(Z) - C_0 \tag{4d}$$

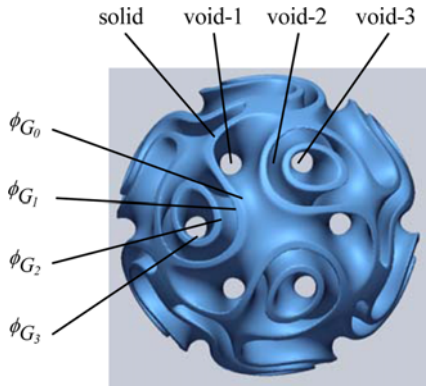

Fig. 4 A sphere-shaped scaffold model with three voids

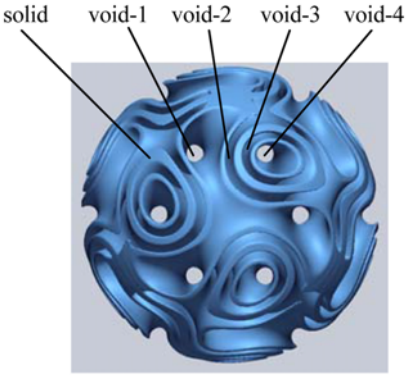

Fig. 5 A sphere-shaped scaffold model with four voids

$$\phi_{G_1} = \sin(X)\cos(Y)+\sin(Z)\cos(X)+\sin(Y)\cos(Z)-C_1 \quad (4e)$$

$$\phi_{G_2} = \sin(X)\cos(Y)+\sin(Z)\cos(X)+\sin(Y)\cos(Z)-C_2 \quad (4f)$$

$$\phi_{G_3} = -[\sin(X)\cos(Y)+\sin(Z)\cos(X)+\sin(Y)\cos(Z)-C_3] \quad (4g)$$

$$\phi_{G_4} = -[\sin(X)\cos(Y)+\sin(Z)\cos(X)+\sin(Y)\cos(Z)-C_4] \quad (4h)$$

$$\phi_{G_5} = -[\sin(X)\cos(Y)+\sin(Z)\cos(X)+\sin(Y)\cos(Z)-C_5] \quad (4i)$$

$$\phi_P = \cos(X)+\cos(Y)+\cos(Z)-C \quad (4j)$$

where ϕ_{G_0}, ϕ_{G_1}, ϕ_{G_2}, ϕ_{G_3}, ϕ_{G_4}, and ϕ_{G_5} are the six TPMS surfaces inflated in normal directions used in the definition of spatial limits of each void. Fig. 5 illustrates the application result of Eq. (4). Of course, it also possible to design various types of scaffold models with different cellular sizes by simply changing the number of unit cells in the calculation, as shown in Fig. 6.

It is worthwhile to note that both conventional TPMS-based scaffolds (i.e., minimal surface network solid scaffolds and minimal surface sheet solid scaffolds) and multi-void TPMS-based scaffolds can be generated in a consistent design framework. That is, we can consider the conventional TPMS-based scaffolds as the special cases of multi-void TPMS-based scaffolds, as shown in Fig. 7. Although we demonstrated here the validity and efficiency of the proposed method through the design of relatively simple spherical and cylindrical

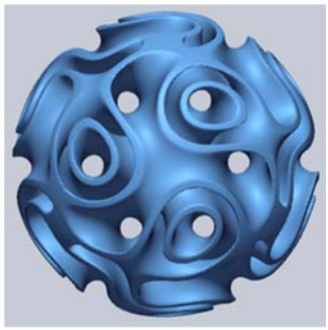

(a) The number of unit cell: 2

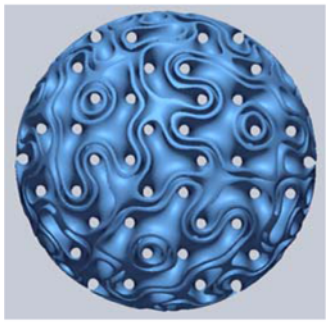

(b) The number of unit cell: 4

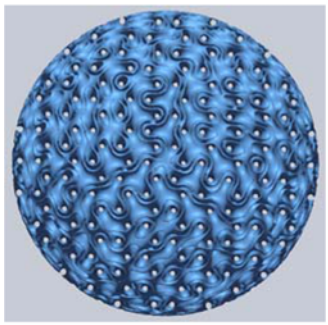

(c) The number of unit cell: 8

Fig. 6 A set of of three-voids scaffold models with different cellular sizes

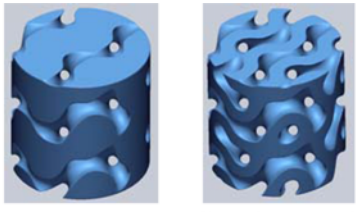

(a) Conventional TPMS-based scaffolds (i.e. network solid scaffold and sheet solid scaffold)

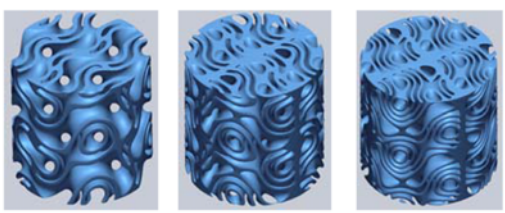

(b) Multi-void TPMS-based scaffolds

Fig. 7 A set of of cylinder-shaped scaffold models with different void numbers

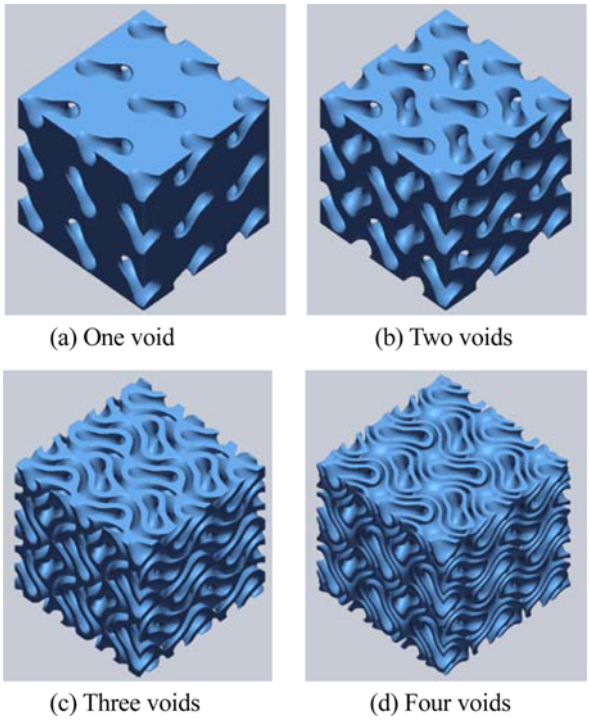

Fig. 8 A set of of box-shaped scaffold models with different void numbers

scaffolds, scaffolds with a large range of external surfaces can be designed by simply varying the DF function for a specific external surface irrespective of the complexity of anatomical models, as shown in Figs. 8~11.

As we know, cells receive oxygen or nutrients by diffusion. Commonly, diffusion rate within a scaffold is known to be mainly related with interconnectivity of pore architecture. In order to show perfect pore interconnectivity of the multi-void TPMS-based scaffold, we visualized internal spaces of a multi-void scaffold with G-surface microarchitecture. As illustrated in Fig. 12, the proposed multi-void scaffold design method is based on the three-dimensionally continuous combination of a set of TPMS surfaces inflated in normal direction to finite thickness. Therefore, the multi-void TPMS-based scaffold has perfect pore interconnectivity in each void. Hence, it enables us to precisely control the proportion of each space according the requirement of a specific application by altering the level constant values of TPMS. Note that the amount of each space can be precisely controlled while maintaining three-dimensionally interconnected-channel geometry. This accurate control of each space would create a suitable environment for cell-matrix and cell-cell interactions, resulting in the self-organization of cells or cell aggregates into multi-material structures with the desired shapes.

In this paper, SA/V ratio is defined as the amount of surface area per unit volume of a scaffold. As shown in Fig. 13, the multi-void TPMS-based scaffold has a high SA/V ratio compared to a conventional TPMS-based scaffold. This means that more cells can be attached on surface of pore for the same volume size of a scaffold while maintaining perfect pore interconnectivity essential for the diffusion of oxygen or nutrients. However, we should reconsider about the definition of SA/V ratio in more detail. If cells are only attached on surface of pore, the

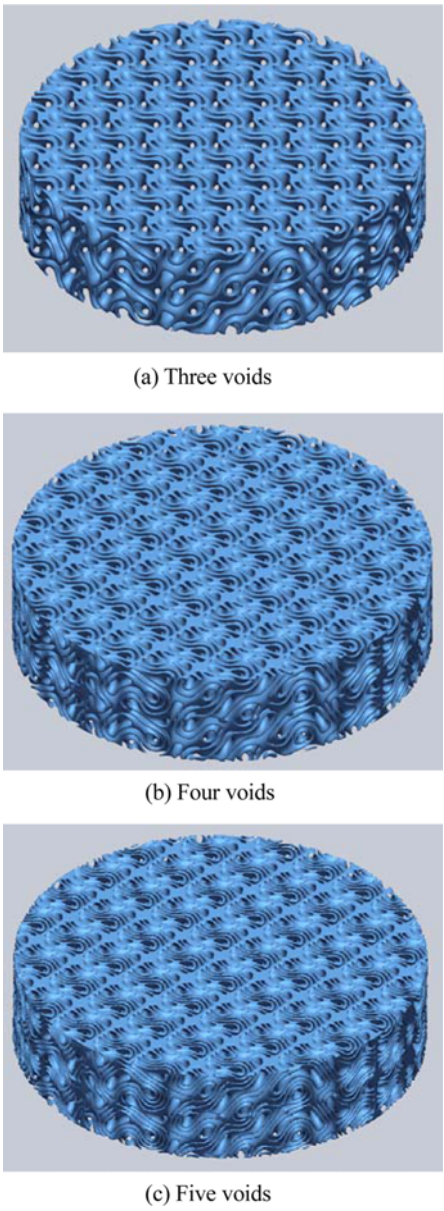

Fig. 9 A set of of disc-shaped scaffold models with different void numbers

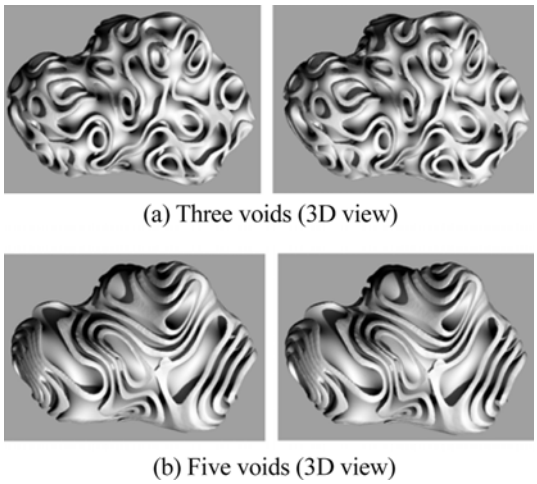

Fig. 10 Talus bone scaffold models with multiple voids

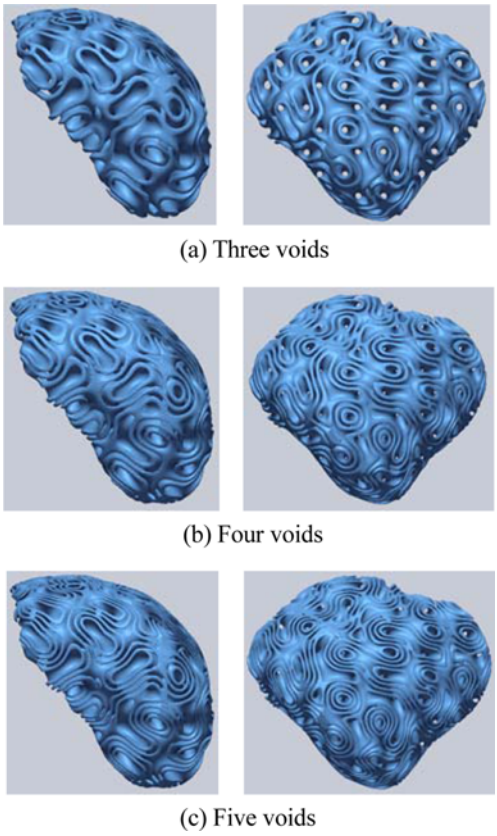

Fig. 11 Liver scaffold models with multiple voids

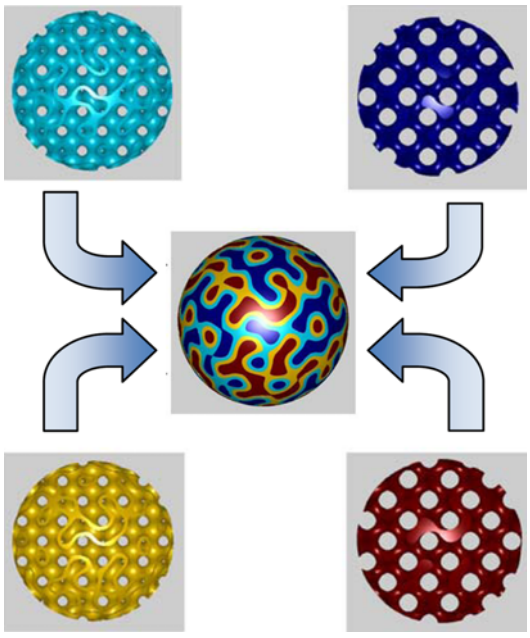

Fig. 12 The proposed multi-void description method based on the three-dimensionally continuous combination of multiple TPMS surfaces inflated in normal direction

volume of cell's space should be dependent on the surface area of scaffold. In this case, change of the void number of TPMS-based scaffold may result in no significant differences in SA/V ratio. On the other hand, if cells are uniformly encapsulated into scaffold volume

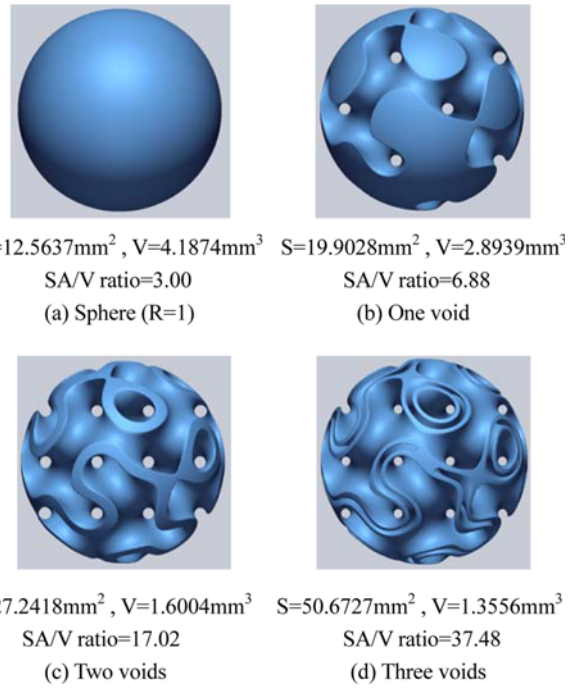

Fig. 13 Variation of SA/V ratio according to the void number

area, SA/V ratio could be changed along with the void number. As aforementioned, specialized organs such as lungs, kidneys, and intestines have high SA/V ratio to increase the surface area available for exchange processes. Principally, the scaffold should be designed by mimicking the structure and biological function of native ECM proteins, which provide mechanical support and regulate cell activities. The pore architecture as well as the nature of a scaffold material was found to control cell adhesion, proliferation, shape and function. With respect to pore microstructure, it is well known that specific surface area and highly porous 3D structure are desirable for high-density cell and tissue cultures.[42,43] Therefore, it can be expected that we will be able to make a tissue or organ more robustly and rapidly when using a scaffold with high SA/V ratio and perfect pore interconnectivity. Although further and detailed *in vitro* and *in vivo* experiments are needed to verify better biological properties of multi-void TPMS-based scaffolds, we can expect that the effect of SA/V ratio on the cell adhesion, migration, and proliferation can be studied more quantitatively and systematically by using the proposed design method.

The proposed multi-void scaffold design algorithm has been implemented using the MATLAB on a PC (Pentium IV, 3 GHz CPU). All the scaffold models were visualized by Geomagic Verify Viewer through STL files. The developed program successfully generated defects free computational models of the porous scaffolds with a variety of TPMS-based cellular microarchitectures. As we can see from the design results, we can easily and fully automatically design various complex porous scaffold digital models through a simple computer program within several minutes.

Recently, advanced 3D printing techniques such as micro-projection stereolithography (μPSL) have been successfully used to fabricate porous scaffolds.[44-49] These techniques can fabricate scaffolds with a large range of structures from nano-meter to mesoscopic scale. It is apparent that further advance of 3D printing process will significantly improve

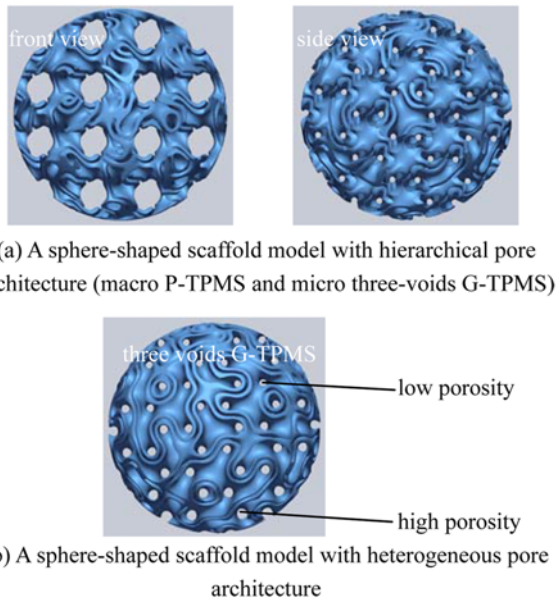

Fig. 14 Hierarchical and functionally graded multi-void TPMS scaffold design

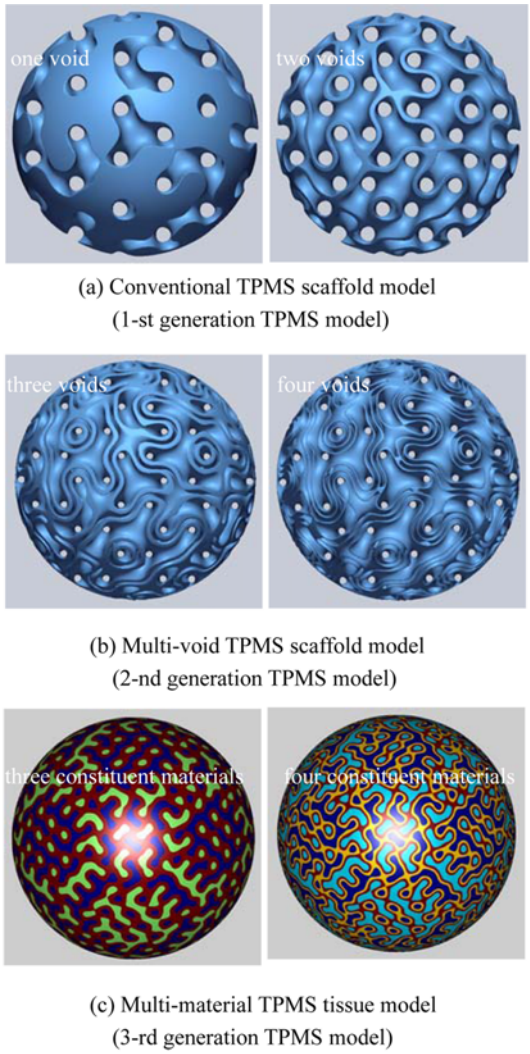

Fig. 15 A variety of computational models of sphere-shaped scaffolds and tissues with G-surface unit cell library

control over the internal pore architectures of porous scaffolds. In the near future, mass production of porous scaffolds with micro- or nano-precision will be possible. Especially in the nanotechnology, the design and fabrication of porous scaffolds with nanoscale pore architectures will dramatically increase the SA/V ratio with unprecedented efficiency. Nanoscale pore architectures are special and interesting because their biological and mechanical properties are different from their macro counterparts. When a porous architecture contains micro- and nanoscale components, size-dependent mechanical properties of constituent materials may play a key role in the enhancement of the overall strength, stiffness and fracture resistance, and need to be incorporated into models to accurately predict the structural response.[50] In this point of view, the proposed multi-void TPMS-based scaffold design method can be considered as one of the promising methods for ideal scaffold design in the era of nanotechnology. The proposed method can provide a general and dynamic design framework thereby making it possible to design pore architectures with a variety of cellular sizes ranging from macroscale to nanoscale by simply controlling the number of unit cells in the calculation (Fig. 6).

The biological structure of a native tissue is inherently heterogeneous and complex. Many natural biological materials have remarkably high strengths when compared with man-made materials of the same composition, yet are able to remain light weight and porous. It is well known that these properties of biological materials arise from the hierarchical arrangement of different structural elements at their relevant length-scales.[50] The proposed multi-void TPMS-based scaffold design method can be easily extended to the more advanced application areas such as functionally graded scaffold design and hierarchical porous scaffold design. The heterogeneous and hierarchical design principles offered by natural biological materials can be applied to create more biomimetic scaffolds and bioartificial tissues using the proposed design method, as shown in Fig. 14.

Recently, another approach to TE has been proposed that does not require a solid scaffold. This process has been termed organ printing or bioprinting. The organ printing can be considered as an extension of the conventional scaffold-based approach that uses 3D printing techniques to build complex scaffold structures. The fundamental concept of organ printing is to fabricate a bioartificial tissue or organ by positioning different materials, such as cells, supporting matrix, and growth factor, etc. in desired locations using 3D printing techniques. By the simultaneous deposition of such biological elements, we can obtain complex organ-like constructs. This scaffold-free approach has a number of potential advantages over scaffold-based approach. The most important advantage is that cells can be cultured in comfortable conditions more similar to the microenvironment of native tissues or organs, thereby resulting in better intercellular communication. Hence, the organ printing can dramatically accelerate and optimize tissue and organ formation. However, the approach faces many challenges, such as the lack of an effective design software that can provide the ability to deliver living cells, supporting matrix, and biomolecules simultaneously in an accurate 3D arrangement. In addition, assembly of large cellular constructs from cell aggregates or cell sheets is limited by the difficulty in transport of oxygen, nutrients, and wastes until a

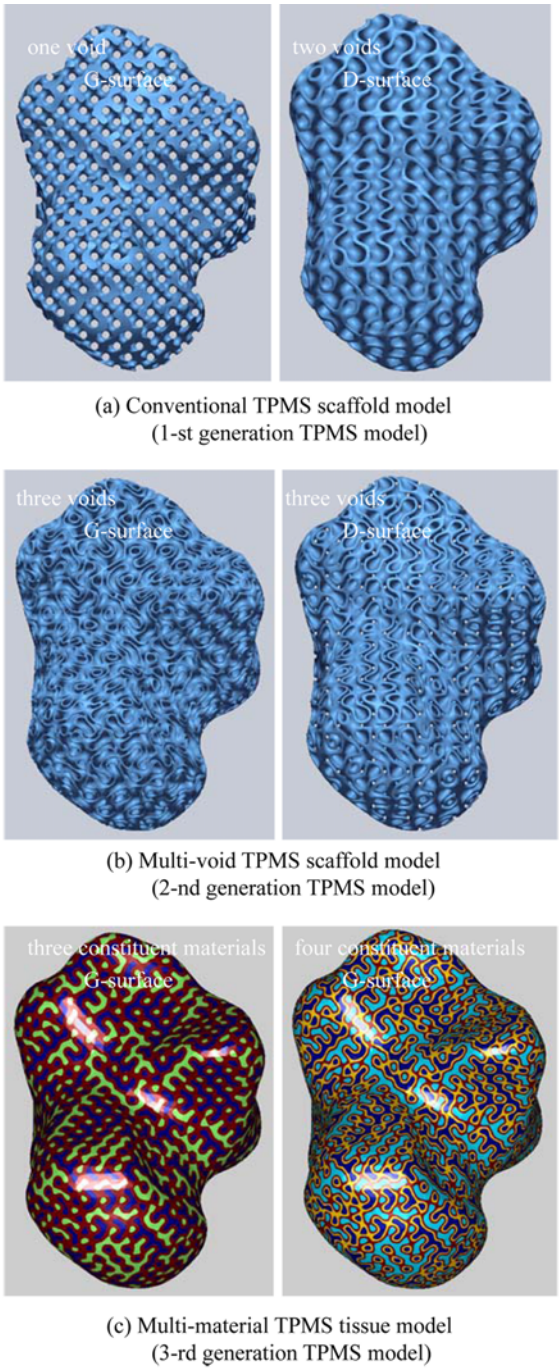

(a) Conventional TPMS scaffold model
(1-st generation TPMS model)

(b) Multi-void TPMS scaffold model
(2-nd generation TPMS model)

(c) Multi-material TPMS tissue model
(3-rd generation TPMS model)

Fig. 16 A variety of computational models of talus bone scaffolds and tissues

vascular network system develops. Therefore, a hybrid approach intermediate to the scaffold-based approach (seeded cells after scaffold fabrication) and scaffold-free approach (organized cellular constructs) that combines advantages of both approaches is likely to be used more popularly. For such an approach, we should develop a general 3D design methodology having multi-space description capability. In this viewpoint, the proposed multi-void TPMS scaffold design method can be considered as one of the plausible solutions.

As shown in Figs. 15 and 16, the proposed design method can be easily extended to the more sophisticated design method for 3D organ printing. That is, TPMS-based pore architecture design method can generate a variety of computational models for prototyping and printing of biomimetic scaffolds and bioartificial organs in an integrated design framework. The conventional TPMS scaffolds of Fig. 15(a) and 16(a) can be thought of as special cases of multi-void TPMS scaffolds of Fig. 15(b) and 16(b). In the same point of view, the multi-void TPMS scaffolds of Fig. 15(b) and 16(b) can be thought of as special cases of multi-material TPMS tissue models of Fig. 15(c) and 16(c). It is very worthwhile to note that TMPS-based pore architecture can provide a general and systematic design framework for generating a variety of computational models ranging from conventional scaffold models, through multi-void scaffold models, to multi-material tissue models.

4. Conclusions and Ideas for Future Research

This study shows that a general design methodology for generating biomimetic scaffolds and structures analogous to tissues can be created by developing an enhanced TPMS pore morphology based on multi-void microarchitecture. The proposed multi-void scaffold design method is able to increase the SA/V ratio of conventional TPMS-based porous scaffolds while maintaining computational efficiency and enhanced interactions with cells. In addition, we could obtain the multi-void TPMS-based scaffold model with fully perfect pore interconnectivity in each void by introducing a three-dimensionally continuous space division method based on a set of inflated TPMS surfaces.

Furthermore, the proposed multi-void TPMS-based scaffold design method can be easily extended to the more advanced application areas, such as functionally graded scaffold design, hierarchical porous scaffold design, and 3D organ printing to create more biomimetic scaffolds and bioartificial tissues. These findings demonstrate that it is possible to generate a variety of computational models ranging from conventional TPMS scaffolds, through multi-void TPMS scaffolds, to multi-material TPMS tissue models in an integrated systematic design framework.

However, more detailed work is needed to demonstrate the full potential of the proposed design method through both *in vitro* and *in vivo* experiments.

ACKNOWLEDGEMENT

This research was supported by Basic Science Research Program through the National Research Foundation of Korea (NRF) funded by the Ministry of Education (No. 2013-R1A1A-2058320).

REFERENCES

1. Starly, B., Lau, W., Bradbury, T., and Sun, W., "Internal Architecture Design and Freeform Fabrication of Tissue Replacement Structures," Computer-Aided Design, Vol. 38, No. 2, pp. 115-124, 2006.

2. Sun, W., Starly, B., Nam, J., and Darling, A., "Bio-CAD Modeling and Its Applications in Computer-Aided Tissue Engineering," Computer-Aided Design, Vol. 37, No. 11, pp. 1097-1114, 2005.

3. Wettergreen, M. A., Bucklen, B. S., Starly, B., Yuksel, E., Sun, W.,

and Liebschner, M. A. K., "Creation of a Unit Block Library of Architectures for Use in Assembled Scaffold Engineering," Computer-Aided Design, Vol. 37, No. 11, pp. 1141-1149, 2005.

4. Tuan, H. S. and Hutmacher, D. W., "Application of Micro CT and Computation Modeling in Bone Tissue Engineering," Computer-Aided Design, Vol. 37, No. 11, pp. 1151-1161, 2005.
5. Naing, M. W., Chua, C. K., Leong, K. F., and Wang, Y., "Fabrication of Customised Scaffolds using Computer-Aided Design and Rapid Prototyping Techniques," Rapid Prototyping Journal, Vol. 11, No. 4, pp. 249-259, 2005.
6. Wang, C. S., Wang, W. H. A., and Lin, M. C., "STL Rapid Prototyping Bio-CAD Model for CT Medical Image Segmentation," Computers in Industry, Vol. 61, No. 3, pp. 187-197, 2010.
7. Cheah, C. M., Chua, C. K., Leong, K. F., and Chua, S. W., "Development of a Tissue Engineering Scaffold Structure Library for Rapid Prototyping. Part 1: Investigation and Classification," The International Journal of Advanced Manufacturing Technology, Vol. 21, No. 4, pp. 291-301, 2003.
8. Cheah, C. M., Chua, C. K., Leong, K. F., and Chua, S. W., "Development of a Tissue Engineering Scaffold Structure Library for Rapid Prototyping. Part 2: Parametric Library and Assembly Program," The International Journal of Advanced Manufacturing Technology, Vol. 21, No. 4, pp. 302-312, 2003.
9. Cheah, C. M., Chua, C. K., Leong, K. F., Cheong, C. H., and Naing, M. W., "Automatic Algorithm for Generating Complex Polyhedral Scaffold Structures for Tissue Engineering," Tissue Engineering, Vol. 10, No. 3-4, pp. 595-610, 2004.
10. Sudarmadji, N., Tan, J. Y., Leong, K. F., Chua, C. K., and Loh, Y. T., "Investigation of The Mechanical Properties and Porosity Relationships in Selective Laser-Sintered Polyhedral for Functionally Graded Scaffolds," Acta Biomaterialia, Vol. 7, No. 2, pp. 530-537, 2011.
11. Sun, W. and Lal, P., "Recent Development on Computer Aided Tissue Engineering-A Review," Computer Methods and Programs in Biomedicine, Vol. 67, No. 2, pp. 85-103, 2002.
12. Sun, W., Starly, B., Darling, A., and Gomez, C., "ComputerAided Tissue Engineering: Application to Biomimetic Modelling and Design of Tissue Scaffolds," Biotechnology and Applied Biochemistry, Vol. 39, No. 1, pp. 49-58, 2004.
13. Chu, W. S., Kim, C. S., Lee, H. T., Choi, J. O., Park, J. I., et al., "Hybrid Manufacturing in Micro/Nano Scale: A Review," Int. J. Precis. Eng. Manuf.-Green Tech., Vol. 1, No. 1, pp. 75-92, 2014.
14. Rajagopalan, S. and Robb, R. A., "Schwarz Meets Schwann: Design and Fabrication of Biomorphic and Durataxic Tissue Engineering Scaffolds," Medical Image Analysis, Vol. 10, No. 5, pp. 693-712, 2006.
15. Melchels, F. P. W., Bertoldi, K., Gabbrielli, R., Velders, A. H., Feijen, J., and Grijpma, D. W., "Mathematically Defined Tissue Engineering Scaffold Architectures Prepared by Stereolithography," Biomaterials, Vol. 31, No. 27, pp. 6909-6916, 2010.
16. Melchels, F. P. W., Barradas, A. M. C., Van Blitterswijk, C. A., De Boer, J., Feijen, J., and Grijpma, D. W., "Effects of the Architecture of Tissue Engineering Scaffolds on Cell Seeding and Culturing," Acta Biomaterialia, Vol. 6, No. 11, pp. 4208-4217, 2010.
17. Yoo, D. J., "Computer-Aided Porous Scaffold Design for Tissue Engineering Using Triply Periodic Minimal Surfaces," Int. J. Precis. Eng. Manuf., Vol. 12, No. 1, pp. 61-71, 2011.
18. Yoo, D. J., "Porous Scaffold Design using the Distance Field and Triply Periodic Minimal Surface Models," Biomaterials, Vol. 32, No. 31, pp. 7741-7754, 2011.
19. Kapfer, S. C., Hyde, S. T., Mecke, K., Arns, C. H., and Schröder-Turk, G. E., "Minimal Surface Scaffold Designs for Tissue Engineering," Biomaterials, Vol. 32, No. 29, pp. 6875-6882, 2011.
20. Yoo, D. J., "Heterogeneous Minimal Surface Porous Scaffold Design using the Distance Field and Radial Basis Functions," Medical Engineering & Physics, Vol. 34, No. 5, pp. 625-639, 2012.
21. Yoo, D. J., "Heterogeneous Porous Scaffold Design for Tissue Engineering using Triply Periodic Minimal Surfaces," Int. J. Precis. Eng. Manuf., Vol. 13, No. 4, pp. 527-537, 2012.
22. Yoo, D. J., "New Paradigms in Internal Architecture Design and Freeform Fabrication of Tissue Engineering Porous Scaffolds," Medical Engineering & Physics, Vol. 34, No. 6, pp. 762-776, 2012.
23. Yoo, D. J., "New Paradigms in Hierarchical Porous Scaffold Design for Tissue Engineering," Materials Science and Engineering: C, Vol. 33, No. 3, pp. 1759-1772, 2013.
24. Yoo, D. J., "Heterogeneous Porous Scaffold Design using the Continuous Transformations of Triply Periodic Minimal Surface Models," Int. J. Precis. Eng. Manuf., Vol. 14, No. 10, pp. 1743-1753, 2013.
25. Schwarz, H., Uber Minimalflachen, Monatsber. Berlin Akad., Apr 1865; Gesammelte Mathematische Abhandlungen, Vol. 1, Springer, Berlin, 1890.
26. Schoen, A. H., "Infinite Periodic Minimal Surfaces without Self-Intersections," NASA Technical Report TN D-5541, 1970.
27. Lord, E. A. and Mackay, A. L., "Periodic Minimal Surfaces of Cubic Symmetry," Current Science, Vol. 85, No. 3, pp. 346-362, 2003.
28. Wohlgemuth, M., Yufa, N., Hoffman, J., and Thomas, E. L., "Triply Periodic Bicontinuous Cubic Microdomain Morphologies by Symmetries," Macromolecules, Vol. 34, No. 17, pp. 6083-6089, 2001.
29. Gandy, P. J. F., Bardhan, S., Mackay, A. L., and Klinowski, J., "Nodal Surface Approximations to the P, G, D and I-WP Triply Periodic Minimal Surfaces," Chemical Physics Letters, Vol. 336, No. 3, pp. 187-195, 2001.
30. Wang, Y., "Periodic Surface Modeling for Computer Aided Nano Design," Computer-Aided Design, Vol. 39, No. 3, pp. 179-189, 2007.

31. Jung, Y., Chu, K. T., and Torquato, S., "A Variational Level Set Approach for Surface Area Minimization of Triply-Periodic Surfaces," Journal of Computational Physics, Vol. 223, No. 2, pp. 711-730, 2007.

32. Yoo, D. J., "Filling Holes in Large Polygon Models using an Implicit Surface Scheme and the Domain Decomposition Method," Int. J. Precis. Eng. Manuf., Vol. 8, No. 1, pp. 3-10, 2007.

33. Yoo, D. J., "Three-Dimensional Morphing of Similar Shapes using a Template Mesh," Int. J. Precis. Eng. Manuf., Vol. 10, No. 1, pp. 55-66, 2009.

34. Yoo, D. J., "Rapid Surface Reconstruction from a Point Cloud using the Least-Squares Projection," Int. J. Precis. Eng. Manuf., Vol. 11, No. 2, pp. 273-283, 2010.

35. Yoo, D. J. and Kwon, H. H., "Shape Reconstruction, Shape Manipulation, and Direct Generation of Input Data from Point Clouds for Rapid Prototyping," Int. J. Precis. Eng. Manuf., Vol. 10, No. 1, pp. 103-113, 2009.

36. Yoo, D. J., "Three-Dimensional Human Body Model Reconstruction and Manufacturing from CT Medical Image Data using a Heterogeneous Implicit Solid Based Approach," Int. J. Precis. Eng. Manuf., Vol. 12, No. 2, pp. 293-301, 2011.

37. Yoo, D. J., "Three-Dimensional Surface Reconstruction of Human Bone using a B-Spline based Interpolation Approach," Computer-Aided Design, Vol. 43, No. 8, pp. 934-947, 2011.

38. Baerentzen, J. A. and Aanaes, H., "Signed Distance Computation using the Angle Weighted Pseudonormal," IEEE Transactions on Visualization and Computer Graphics, Vol. 11, No. 3, pp. 243-253, 2005.

39. Guezlec, A., ""Meshsweeper": Dynamic Point-to-Polygonal Mesh Distance and Applications," IEEE Transactions on Visualization and Computer Graphics, Vol. 7, No. 1, pp. 47-61, 2001.

40. Sud, A., Otaduy, M. A., and Manocha, D., "DiFi: Fast 3D Distance Field Computation using Graphics Hardware," Proc. of Computer Graphics Forum, Vol. 23, No. 3, pp. 557-566, 2004.

41. Yoo, D. J., "General 3D Offsetting of a Triangular Net using an Implicit Function and the Distance Fields," Int. J. Precis. Eng. Manuf., Vol. 10, No. 4, pp. 131-142, 2009.

42. Min, B. M., Lee, G., Kim, S. H., Nam, Y. S., Lee, T. S., and Park, W. H., "Electrospinning of Silk Fibroin Nanofibers and Its Effect on the Adhesion and Spreading of Normal Human Keratinocytes and Fibroblasts in Vitro," Biomaterials, Vol. 25, No. 7, pp. 1289-1297, 2004.

43. Chen, C. S., Mrksich, M., Huang, S., Whitesides, G. M., and Ingber, D. E., "Geometric Control of Cell Life and Death," Science, Vol. 276, No. 5317, pp. 1425-1428, 1997.

44. Sun, C., Fang, N., Wu, D., and Zhang, X., "Projection Micro-Stereolithography Using Digital Micro-Mirror Dynamic Mask," Sensors and Actuators A: Physical, Vol. 121, No. 1, pp. 113-120, 2005.

45. Lu, Y., Mapili, G., Suhali, G., Chen, S., and Roy, K., "A Digital MicroMirror Devicebased System for the Microfabrication of Complex, Spatially Patterned Tissue Engineering Scaffolds," Journal of Biomedical Materials Research Part A, Vol. 77, No. 2, pp. 396-405, 2006.

46. Park, I. B., Ha, Y. M., Kim, M. S., and Lee, S. H., "Fabrication of a Micro-Lens Array with a Nonlayered Method in Projection Microstereolithography," Int. J. Precis. Eng. Manuf., Vol. 11, No. 3, pp. 483-490, 2010.

47. Jung, J. W., Kang, H.-W., Kang, T.-Y., Park, J. H., Park, J., and Cho, D.-W., "Projection Image-Generation Algorithm for Fabrication of a Complex Structure using Projection-based Microstereolithography," Int. J. Precis. Eng. Manuf., Vol. 13, No. 3, pp. 445-449, 2012.

48. Gauvin, R., Chen, Y. C., Lee, J. W., Soman, P., Zorlutuna, P., et al., "Microfabrication of Complex Porous Tissue Engineering Scaffolds using 3D Projection Stereolithography," Biomaterials, Vol. 33, No. 15, pp. 3824-3834, 2012.

49. Dean, D., Wallace, J., Siblani, A., Wang, M. O., Kim, K., et al., "Continuous Digital Light Processing (cDLP): Highly Accurate Additive Manufacturing of Tissue Engineered Bone Scaffolds: This Paper Highlights the Main Issues Regarding the Application of Continuous Digital Light Processing (cDLP) for the Production of Highly Accurate PPF Scaffolds with Layers as thin as 60 m for Bone Tissue Engineering," Virtual and Physical Prototyping, Vol. 7, No. 1, pp. 13-24, 2012.

50. Jang, D., Meza, L. R., Greer, F., and Greer, J. R., "Fabrication and Deformation of Three-Dimensional Hollow Ceramic Nanostructures," Nature Materials, Vol. 12, No. 10, pp. 893-898, 2013.